Sea level rise from Antarctic collapse may be slower than suggested

Impact on sea level of Antarctic ice sheet collapse

Summary: A new study by scientists in the UK and France has found that Antarctic ice sheet collapse will have serious consequences for sea level rise over the next two hundred years, though not as much as some have suggested.

This study uses an ice-sheet model to predict the consequences of unstable retreat of the ice, which recent studies suggest has begun in West Antarctica. Scientists, led by Catherine Ritz from Université Grenoble Alpes in France and Tamsin Edwards from The Open University, predict that the contribution is most likely to be 10 cm of sea-level rise this century under a mid- to high-climate scenario, but is extremely unlikely to be higher than 30 cm. When combined with other contributions, that's a significant challenge for adapting to future sea level rise. But it's also far lower than some previous estimates, which were as high as 1 meter from Antarctica alone.

The study's central estimate raises the Intergovernmental Panel on Climate Change (IPCC) central prediction of 60 cm global sea-level rise by just a few centimeters under the mid to high scenario they used. But the UK and France team's method allowed them to assess the likelihood of sea-level rise from substantial parts of the ice sheet collapsing, which the IPCC could not due to a lack of evidence. They predict there is a one in twenty chance that Antarctic collapse could contribute more than 30 cm sea-level rise by the end of the century and more than 72 cm by 2200. This does not rule out larger contributions on longer time scales.

Their method is more comprehensive than previous estimates, because it has more exploration of uncertainty than previous model predictions and more physics than those based on extrapolation or expert judgment.

The paper 'Potential sea-level rise from Antarctic ice sheet instability constrained by observations' is published on 18th November, 2015 in the academic journal *Nature*.

pdf reprint follows................

LETTER

Potential sea–level rise from Antarctic ice–sheet instability constrained by observations

Catherine Ritz[1,2]*, Tamsin L. Edwards[3,4]*, Gaël Durand[1,2], Antony J. Payne[4], Vincent Peyaud[1,2] & Richard C. A. Hindmarsh[5]

Large parts of the Antarctic ice sheet lying on bedrock below sea level may be vulnerable to marine-ice-sheet instability (MISI)[1], a self-sustaining retreat of the grounding line triggered by oceanic or atmospheric changes. There is growing evidence[2–4] that MISI may be underway throughout the Amundsen Sea embayment (ASE), which contains ice equivalent to more than a metre of global sea-level rise. If triggered in other regions[5–8], the centennial to millennial contribution could be several metres. Physically plausible projections are challenging[9]: numerical models with sufficient spatial resolution to simulate grounding-line processes have been too computationally expensive[2,3,10] to generate large ensembles for uncertainty assessment, and lower-resolution model projections[11] rely on parameterizations that are only loosely constrained by present day changes. Here we project that the Antarctic ice sheet will contribute up to 30 cm sea-level equivalent by 2100 and 72 cm by 2200 (95% quantiles) where the ASE dominates. Our process-based, statistical approach gives skewed and complex probability distributions (single mode, 10 cm, at 2100; two modes, 49 cm and 6 cm, at 2200). The dependence of sliding on basal friction is a key unknown: nonlinear relationships favour higher contributions. Results are conditional on assessments of MISI risk on the basis of projected triggers under the climate scenario A1B (ref. 9), although sensitivity to these is limited by theoretical and topographical constraints on the rate and extent of ice loss. We find that contributions are restricted by a combination of these constraints, calibration with success in simulating observed ASE losses, and low assessed risk in some basins. Our assessment suggests that upper-bound estimates from low-resolution models and physical arguments[9] (up to a metre by 2100 and around one and a half by 2200) are implausible under current understanding of physical mechanisms and potential triggers.

It is not yet clear[9] whether human-induced climate change has influenced the circulation of warm Circumpolar Deep Water driving grounding-line retreat[4] of Pine Island Glacier, Thwaites Glacier and other glaciers in the ASE, or how this circulation might change in future[9]. However, grounding-line retreat under MISI is proposed to occur at a rate more or less independent of the original trigger and may continue even if that trigger diminishes[2]. MISI can be limited by buttressing from ice shelves or specific configurations of bedrock topography[1,12] and possibly also higher friction at the bed[2,13,14]. It has been suggested that grounding-line retreat could continue in the ASE for decades[2] to centuries[3,4] owing to weak topographical constraints, possibly slowed in Pine Island Glacier by a region of higher friction behind the grounding line[2,13,14]. MISI could be triggered elsewhere by ice-shelf collapse and/or exposure of further ice shelves to Circumpolar Deep Water, both of which are projected in some regions[6,7] under the Special Report on Emissions Scenarios (SRES) A1B climate scenario[9]. Here we aim to quantify the dynamic contribution of the Antarctic ice sheet to sea level in the event of MISI under A1B.

We take a statistical–physical approach, using a numerical ice-sheet model[15] supplemented by statistical modelling of the probability of MISI onset. The statistical modelling represents the ocean and atmospheric drivers of MISI and the response of ice shelves, which are poorly known owing to the modelling challenges described earlier. We assign probabilities of MISI onset as a function of time until 2200 in each of 11 sectors (Extended Data Fig. 1a) using expert synthesis of observed grounding-line retreat and thinning[4,16,17] and projected ice-shelf basal[6,18] and surface[7] melting under A1B.

The response of the grounding-line position to MISI onset is represented with a new parameterization: if a MISI trigger occurs in a sector, the potential rate of retreat is a function of the basal friction coefficient at each part of the current grounding line (Extended Data Fig. 2c–e), with the form of the dependence (Extended Data Fig. 1b) based on theoretical considerations[1]. Grounding-line response is modified by two ice dynamical conditions that allow retreat to occur only if bedrock is downsloping from the margin (but allowing retreat over small bumps) and only at a rate not exceeding the theoretical limit[1]. The response is also modified by the basal friction law—the relationship between basal friction and sliding velocity—which has three possible configurations in this study: linear–viscous, nonlinear Weertman, or plastic flow.

To assess modelling uncertainties, we generated a 3,000-member ensemble sampling MISI onset dates in the 11 sectors, 3 parameters governing retreat rate, bedrock topography, and the form of the basal friction law. We weighted the ensemble members in a Bayesian statistical framework with the difference between simulated and observed mass losses in the ASE (the only region where grounding-line retreat has been observed) to obtain calibrated projections. Details and projections are in Supplementary Information.

Observational calibration gives greatest weight to the ensemble members that most successfully simulate present day ASE mass loss. The expected mass trend from 1992 to 2011 is $-59.0 \pm 13.5\,\mathrm{Gt\,yr^{-1}}$, where the standard deviation is dominated by a conservative tolerance for model error (Supplementary Information, section 1.7). The range of simulated mass trends is -13.4 to $-218.3\,\mathrm{Gt\,yr^{-1}}$, with 39% of the ensemble more than three standard deviations from the expected trend, of which nearly all simulate losses that are too large. Parameter values that generate the most rapid and widespread present day retreat in the ASE are thus effectively ruled out. These also tend to give the highest sea-level projections, so calibration decreases projected quantiles. Medians at 2100 and 2200 decrease by 33% and 20%, and 95% quantiles by 36% and 30%, respectively; the modes, however, increase, particularly at 2200 owing to a shift in density from one local mode to the other.

Spatial patterns of the probability of ungrounding (Fig. 1) show how local bed elevation, slope and friction strongly modulate the response to MISI onset. We find that the region with the highest probability of ungrounding and sea-level contribution is the ASE, owing to the
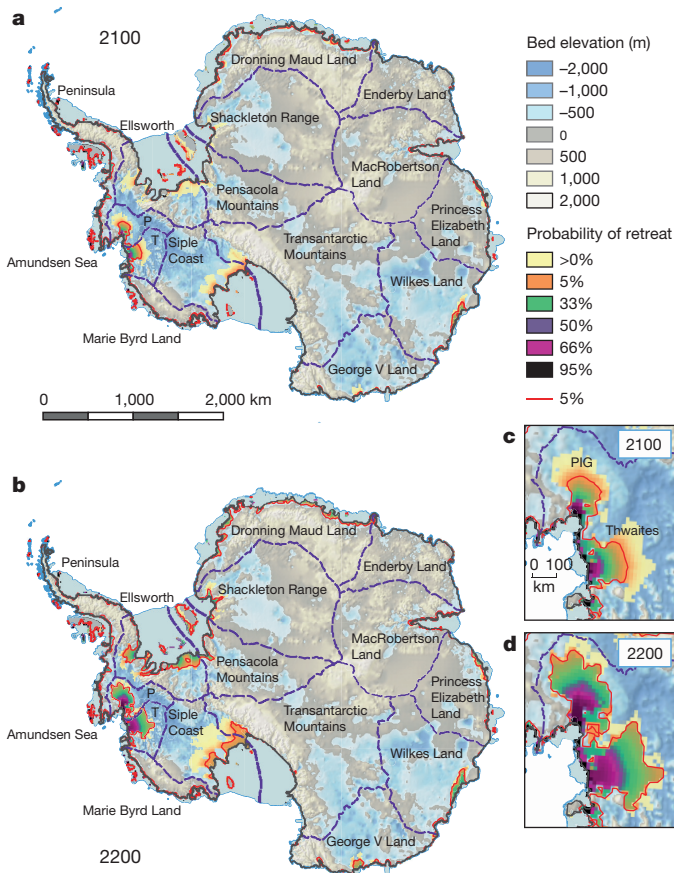
Figure 1 | Projected grounding-line retreat. a, b, Probability density estimates of grounding-line retreat at 2100 (**a**) and 2200 (**b**), overlaid on bedrock topography[24]. Red lines show 0.05 contour: an estimated 95% probability that retreat will be less extensive than this. **c, d,** ASE with Pine Island (PIG) and Thwaites glaciers.

combination of topography (downsloping bedrock below sea level) and low friction (Extended Data Fig. 2c–e). Our 95% quantiles for the ASE are 25 cm at 2100 and 48 cm at 2200 (all values are sea-level equivalent and, unless specified otherwise, 95% quantiles). The Thwaites region, which includes the Smith and Kohler glaciers[4], contributes the greater part of this: 58% at 2100 and 53% at 2200. This is partly due to the basin definition, but is also due to relatively rapid and substantial thinning of Thwaites upstream of the grounding line (see Supplementary Video 1). The Peninsula and Marie Byrd Land hardly respond, despite being assigned the same probabilities of onset as the ASE

(owing to observed grounding-line retreat and thinning[4,16,17]), because their bedrock is largely above sea level.

Although basin contributions depend partly on coastline length, similar topographical limits are seen elsewhere: on the basis of projected ice-shelf surface and basal melting[7,18], Princess Elizabeth Land and MacRobertson Land are assigned substantial probabilities of MISI but contribute only 1 cm by 2200, while Dronning Maud Land is assigned lower probabilities but contributes up to 4 cm by 2100 and 8 cm by 2200. Responses also vary across the three basins of the Ronne–Filchner sector, which are assigned identical onset dates on the basis of projected Circumpolar Deep Water intrusion[6]. Ellsworth shows widespread ungrounding, with the 95% quantile at 2200 approximately delineating a previously deglaciated region[19] (Fig. 1 and Extended Data Fig. 3a), and contributes 9 cm by 2200; Shackleton Range and Pensacola Mountains show much less retreat and contribute 6 cm and 4 cm, respectively.

For Totten Glacier in Wilkes Land, our results suggest that if current dynamic thinning is MISI driven by Circumpolar Deep Water[8], the region has some potential for ungrounding (up to 5 cm by 2200). The Siple Coast is assigned a small probability from ice-shelf basal melting[18] but, when triggered, ungrounding is widespread owing to low basal friction (Extended Data Fig. 2c); we estimate that the total risk is small (up to 3 cm by 2200). These constraints are not absolute bounds—greater deglaciation has occurred in the past over longer time scales[9]—but appear to limit the amount of ice that can be lost in two centuries. Extended Data Figure 4 illustrates the effects of the two ice dynamical conditions, for example in George V Land, which is thought to be vulnerable in the long term[5] (Supplementary Information, section 2.2.1).

The total continental contribution to sea level is relatively low in the first century and accelerates in the second (Fig. 2a), although a second mode emerges at 6 cm by 2200 (Fig. 2b). The probability of exceeding 10 cm rises rapidly this century to 57% at 2100; for exceeding half a metre, it reaches only 33% at 2200 (Fig. 2c, d).
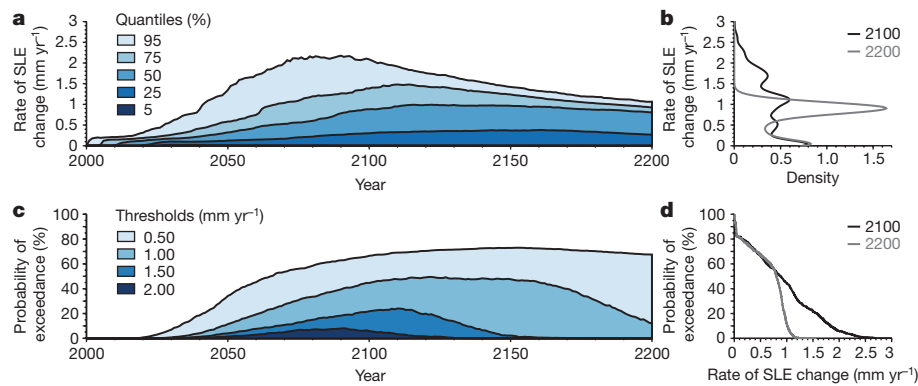
We find that the rate of sea-level rise from the ASE could be substantial this century: up to 1.3 mm yr^{-1} by 2050 and 2.1 mm yr^{-1} by 2100 (Fig. 3). However, many simulations stop (near zero mode at 2100 and local mode at 2200; Fig. 3b) or slow their retreat, particularly those with a linear–viscous friction law, so the 95% quantile at 2200 (1.1 mm yr^{-1}) is half that at 2100. Narrow zones of higher friction (hard bedrock) situated a few tens of kilometres upstream impede further retreat (Extended Data Fig. 3b). Extended Data Figure 5 shows this and other threshold behaviour dependent on friction law.

The strong dependence of ASE response on basal friction law lies behind the bimodal projections for Antarctica at 2200 (Extended Data Fig. 6). Projections of MISI using one friction law[2,3,10] may systematically under- or overestimate sea-level rise and will almost certainly underestimate its uncertainty. Although the sensitivity of
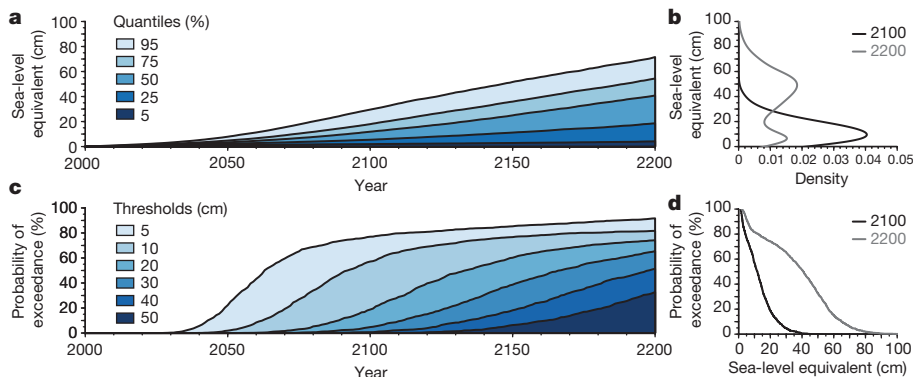
Figure 2 | Projected sea-level rise. a, Quantiles of Antarctic dynamic mass losses in cm sea-level equivalent as a function of time. **b,** Probability densities at 2100 and 2200. **c,** Probabilities of exceeding particular thresholds as a function of time. **d,** Probability of exceeding any threshold at 2100 and 2200.

Figure 3 | Projected rate of sea-level rise from the Amundsen Sea.
a, Quantiles of the rate of ASE dynamic mass losses in mm yr^{-1} sea-level equivalent (SLE) as a function of time. **b**, Probability densities at 2100 and 2200. **c**, Probabilities of exceeding particular thresholds as a function of time. **d**, Probability of exceeding any threshold at 2100 and 2200.

grounding-line migration to friction law has been explored previously[2,13,14], a fully Bayesian approach allows us to quantify the probabilistic contribution to uncertainty in sea-level rise. Extensive observations of basal type and hydrology, and better theoretical understanding of basal hydrology and sliding, would be needed to reduce this uncertainty.

Sensitivity to onset probabilities is limited for most basins by glaciological constraints that slow or stop retreat (Supplementary Information, section 2.2.2). Altering retreat onset probabilities by ± 20% changes basin 95% quantiles at 2200 by up to about 1 cm, and using early or late ASE onset dates (2000–2010 or 2020–2030) changes the 95% quantile at 2200 by less than 2 cm (Extended Data Fig. 9a). Only Shackleton, Siple Coast and Transantarctic Mountains (Extended Data Fig. 9b–d) approach a linear response; increasing Siple Coast onset probabilities tenfold increases the 95% quantile at 2200 by 8 cm.

Observational calibration reduces projected quantiles by constraining the maximum rate of retreat and the regions over which this can occur (Extended Data Figs 7 and 8), mainly in the ASE. It presupposes that the best parameter values in one region are the best everywhere (although not the sliding law, which is not calibrated because it varies spatially; Supplementary Information, section 1.7). To assess the effect of this, we estimate that calibrating only the ASE contribution would increase 95% quantiles by approximately 6 cm (22%) at 2100 and 21 cm (29%) at 2200. Results are robust to other calibration choices (95% quantiles at 2200 vary by a few centimetres; Supplementary Information, section 2.2.4).

Our results are consistent with regional high-resolution model projections. In particular, projected ice losses by 2200 under A1B driven by one of the ocean simulations on which we base our onset probabilities[10] lie within our uncertainty estimates for the ASE (19–30% quantiles), Ronne–Filchner (Ellsworth, Pensacola Mountains, Shackleton: 56–65% quantiles) and Ross basins (Siple Coast, Transantarctic Mountains: 90%; tenfold Siple Coast probabilities 80%). For Marie Byrd Land, the high-resolution projections are lower than our ensemble, but the contribution to our result is less than a centimetre. Projected rates for Pine Island and Thwaites glaciers are also consistent with high-resolution modelling under idealized basal melting scenarios, and continental totals with a statistically based projection assuming ASE collapse in 2012 and linear growth of ice discharge elsewhere[20] (Supplementary Information, section 2.1).

Our projections are essentially incompatible with upper-bound estimates for MISI[9,21] of around 50–80 cm by 2100 and 140 cm by 2200 derived from physical arguments, extrapolation or low-resolution numerical models, and around 1 m by 2100 (95% quantile) from expert elicitation[22]. Half a metre of sea level rise by 2100 is not exceeded at the 99.9% quantile (uncalibrated: 98% percentile). Contributions of around 1 metre by 2100 were obtained (Extended Data Fig. 10 and

Supplementary Information, section 2.2.3) by setting the parameter values to maximize ice loss and additionally either violating the theoretical limit or triggering immediate MISI everywhere (in 2000 for the Peninsula, ASE and Marie Byrd Land; 2020 elsewhere), but we do not consider these realistic. One metre by 2200 is exceeded at the 99.9% quantile (uncalibrated: 95% percentile).

We therefore find that MISI in the ASE could drive large and rapid sea-level rise but that the total Antarctic contribution is moderated by important physical constraints. Large uncertainties remain, in particular basal friction and its evolution, and further observations of surface and grounding-line changes would improve initialization and calibration. Future advances (high-resolution simulation of the ice-sheet–ice-shelf–ocean system; increased computational resources) will improve representation of the processes we parameterize and allow ensemble methods, while comparing multiple models would explore other representations of ice dynamics. But, given current understanding, our results indicate that plausible predictions of Antarctic ice-sheet instability leading to greater than around half a metre of sea-level rise by 2100 or twice that by 2200 would require new physical mechanisms[23], new projections of MISI triggers, or both.

1. Schoof, C. Ice sheet grounding line dynamics: steady states, stability, and hysteresis. *J. Geophys. Res.* **112,** F03S28 (2007).
2. Favier, L. *et al.* Retreat of Pine Island Glacier controlled by marine ice-sheet instability. *Nature Clim. Chang.* **5,** 1–5 (2014).
3. Joughin, I., Smith, B. E. & Medley, B. Marine ice sheet collapse potentially under way for the Thwaites Glacier Basin, West Antarctica. *Science* **344,** 735–738 (2014).
4. Rignot, E., Mouginot, J., Morlighem, M., Seroussi, H. & Scheuchl, B. Widespread, rapid grounding line retreat of Pine Island, Thwaites, Smith, and Kohler glaciers, West Antarctica, from 1992 to 2011. *Geophys. Res. Lett.* **41,** 3502–3509 (2014).
5. Mengel, M. & Levermann, A. Ice plug prevents irreversible discharge from East Antarctica. *Nature Clim. Chang.* **4,** 451–455 (2014).
6. Hellmer, H. H., Kauker, F., Timmermann, R., Determann, J. & Rae, J. Twenty-first-century warming of a large Antarctic ice-shelf cavity by a redirected coastal current. *Nature* **485,** 225–228 (2012).
7. Kuipers Munneke, P., Ligtenberg, S. R. M., Van den Broeke, M. R. & Vaughan, D. G. Firn air depletion as a precursor of Antarctic ice-shelf collapse. *J. Glaciol.* **60,** 205–214 (2014).
8. Khazendar, A., Schodlok, M. P., Fenty, I., Ligtenberg, S. R. M., Rignot, E. & Van Den Broeke, M. R. Observed thinning of Totten Glacier is linked to coastal polynya variability. *Nature Commun.* **4,** 2857 (2013).
9. Intergovernmental Panel on Climate Change. *Working Group I Contribution to the IPCC Fifth Assessment Report Climate Change 2013: The Physical Science Basis* (Cambridge Univ. Press, 2013).
10. Cornford, S. L. *et al.* Century-scale simulations of the response of the West Antarctic Ice Sheet to a warming climate. *Cryosphere* **9,** 1579–1600 (2015).
11. Levermann, A. *et al.* Projecting Antarctic ice discharge using response functions from SeaRISE ice-sheet models. *Earth Syst. Dynam.* **5,** 271–293 (2014).

12. Gudmundsson, G. H., Krug, J., Durand, G., Favier, L. & Gagliardini, O. The stability of grounding lines on retrograde slopes. *Cryosphere* **6,** 1497–1505 (2012).
13. Joughin, I. *et al.* Basal conditions for Pine Island and Thwaites Glaciers, West Antarctica, determined using satellite and airborne data. *J. Glaciol.* **55,** 245–257 (2009).
14. Joughin, I., Smith, B. E. & Holland, D. M. Sensitivity of 21st century sea level to ocean-induced thinning of Pine Island Glacier, Antarctica. *Geophys. Res. Lett.* **37,** L20502 (2010).
15. Ritz, C., Rommeleare, V. & Dumas, C. Modeling the evolution of Antarctic ice sheet over the last 420,000 years: implications for altitude changes in the Vostok region. *J. Geophys. Res.* **106,** 31943–31964 (2001).
16. Pritchard, H. D., Arthern, R. J., Vaughan, D. G. & Edwards, L. A. Extensive dynamic thinning on the margins of the Greenland and Antarctic ice sheets. *Nature* **461,** 971–975 (2009).
17. Park, J. W. *et al.* Sustained retreat of the Pine Island Glacier. *Geophys. Res. Lett.* **40,** 2137–2142 (2013).
18. Timmermann, R. & Hellmer, H. H. Southern Ocean warming and increased ice shelf basal melting in the twenty-first and twenty-second centuries based on coupled ice-ocean finite-element modelling. *Ocean Dyn.* **63,** 1011–1026 (2013).
19. Ross, N. *et al.* Steep reverse bed slope at the grounding line of the Weddell Sea sector in West Antarctica. *Nature Geosci.* **5,** 393–396 (2012).
20. Little, C. M., Oppenheimer, M. & Urban, N. M. Upper bounds on twenty-first-century Antarctic ice loss assessed using a probabilistic framework. *Nature Clim. Chang.* **3,** 654–659 (2013).
21. Katsman, C. A. *et al.* Exploring high-end scenarios for local sea level rise to develop flood protection strategies for a low-lying delta—the Netherlands as an example. *Clim. Change* **109,** 617–645 (2011).
22. Bamber, J. L. & Aspinall, W. P. An expert judgement assessment of future sea level rise from the ice sheets. *Nature Clim. Chang.* **3,** 424–427 (2013).
23. Pollard, D., Deconto, R. M. & Alley, R. B. Potential Antarctic Ice Sheet retreat driven by hydrofracturing and ice cliff failure. *Earth Planet. Sci. Lett.* **412,** 112–121 (2015).
24. Le Brocq, A. M., Payne, A. J. & Vieli, A. An improved Antarctic dataset for high resolution numerical ice sheet models (ALBMAP v1). *Earth Syst. Sci. Data* **2,** 247–260 (2010).

**Supplementary Information** is available in the online version of the paper.

Author Contributions C.R. and V.P. worked on the development of the GRISLI model and did the numerical modelling. C.R. and G.D., with contributions from T.L.E., performed the physics analysis. T.L.E. designed the experiments with contributions from all authors, wrote the manuscript with contributions from C.R. and G.D., and performed the statistical analysis. T.L.E. and C.R. produced the figures and animation, with contributions from G.D. The sampling and geostatistical analysis were produced by A.J.P., and the theoretical conditions of grounding-line retreat were developed by R.A.H., C.R. and G.D.

Author Information Reprints and permissions information is available at www.nature.com/reprints. The authors declare no competing financial interests. Readers are welcome to comment on the online version of the paper. Correspondence and requests for materials should be addressed to T.L.E. (tamsin.edwards@open.ac.uk).
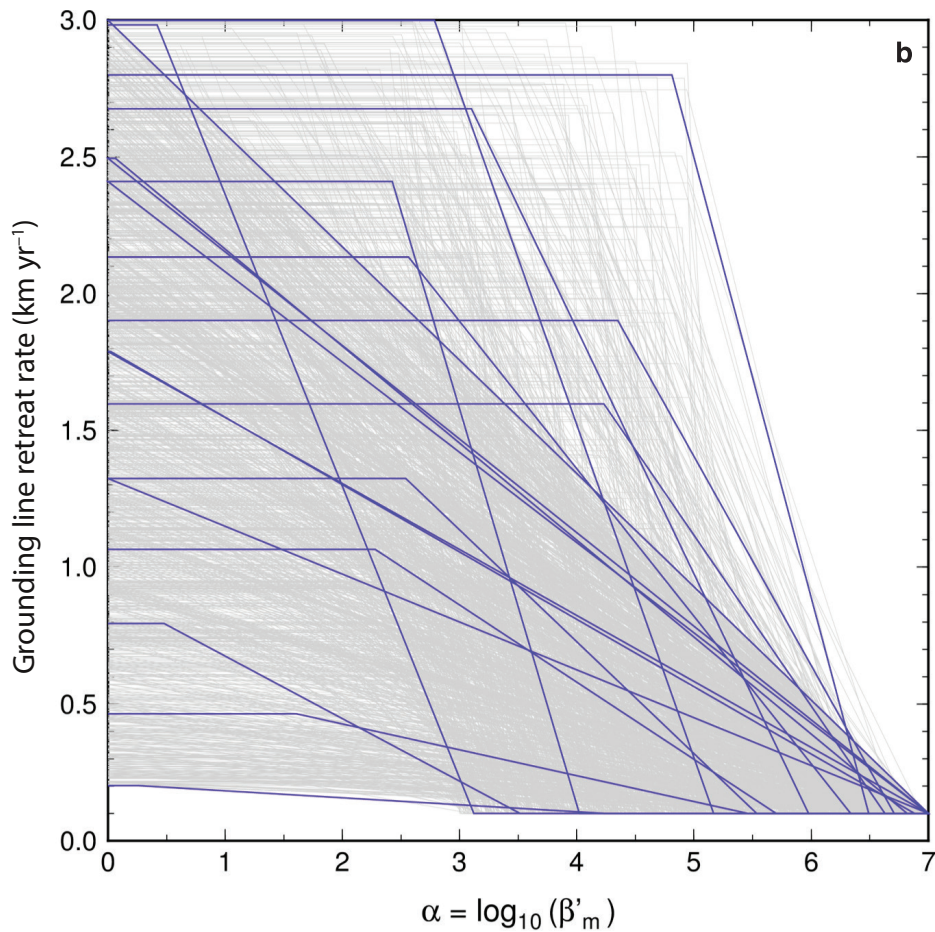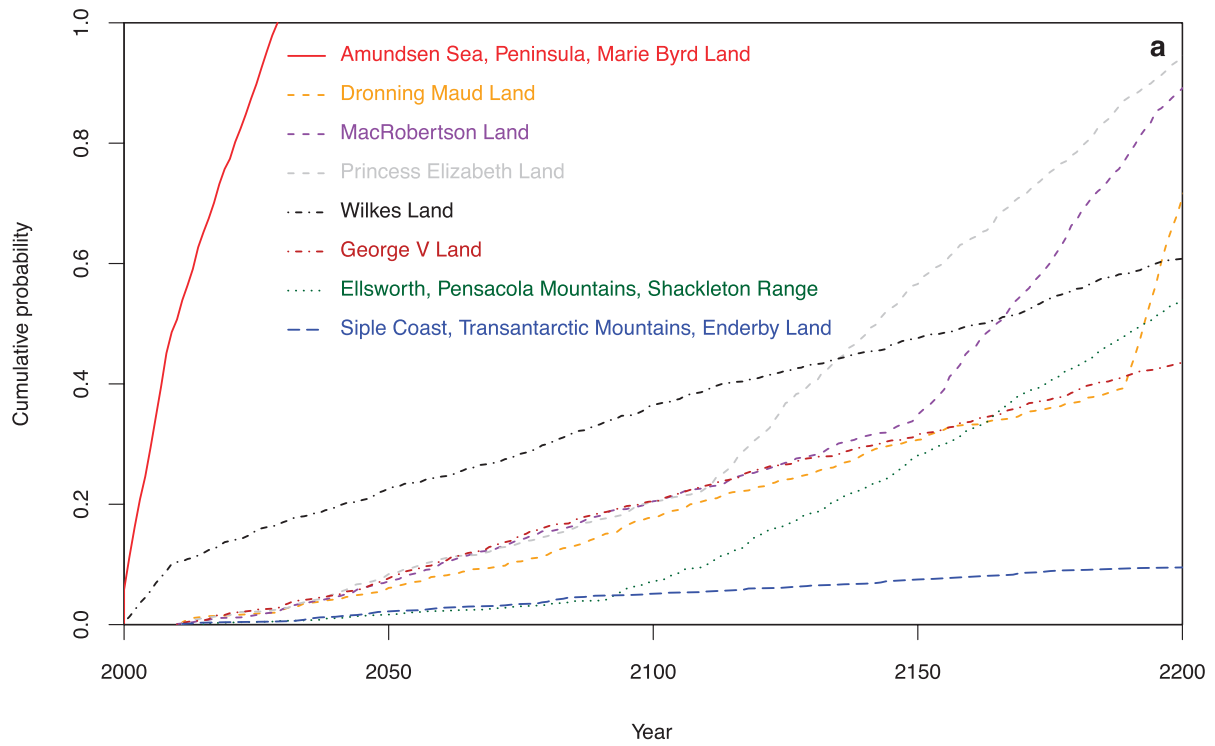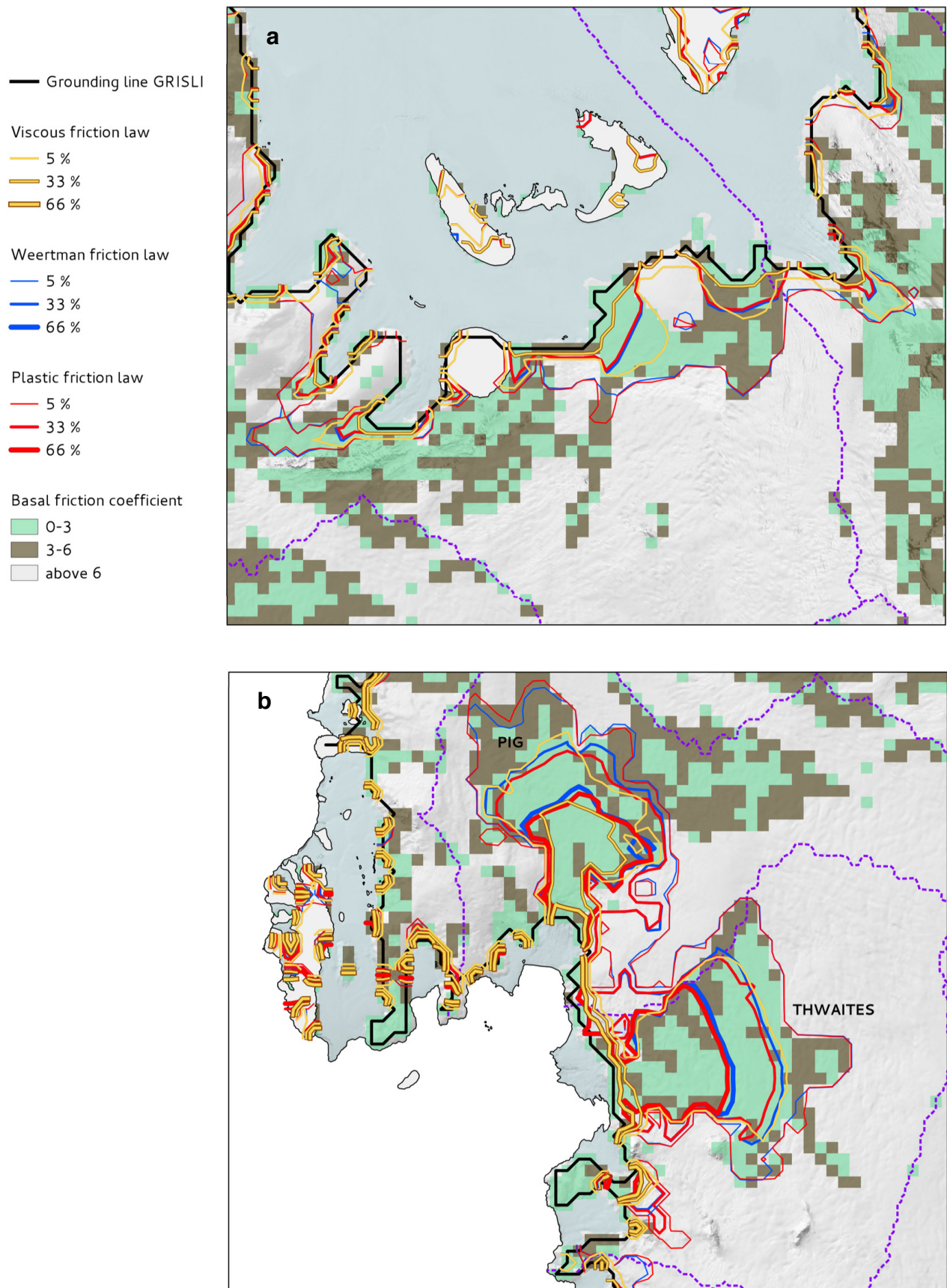
Extended Data Figure 1 | Grounding-line retreat parameterization.
a, Cumulative probability distributions of MISI onset for 14 basins
(Fig. 1) aggregated into 11 independent sectors. **b**, Piecewise linear
parameterization prescribing the dependence of grounding-line retreat
rate on the logarithm of the effective basal friction coefficient (Extended
Data Fig. 2). Each of the 1,000 functional forms is a variant used in the
ensemble; a subset are shown in bold as examples. See also Supplementary
Information, sections 1.6.1, 1.6.2.
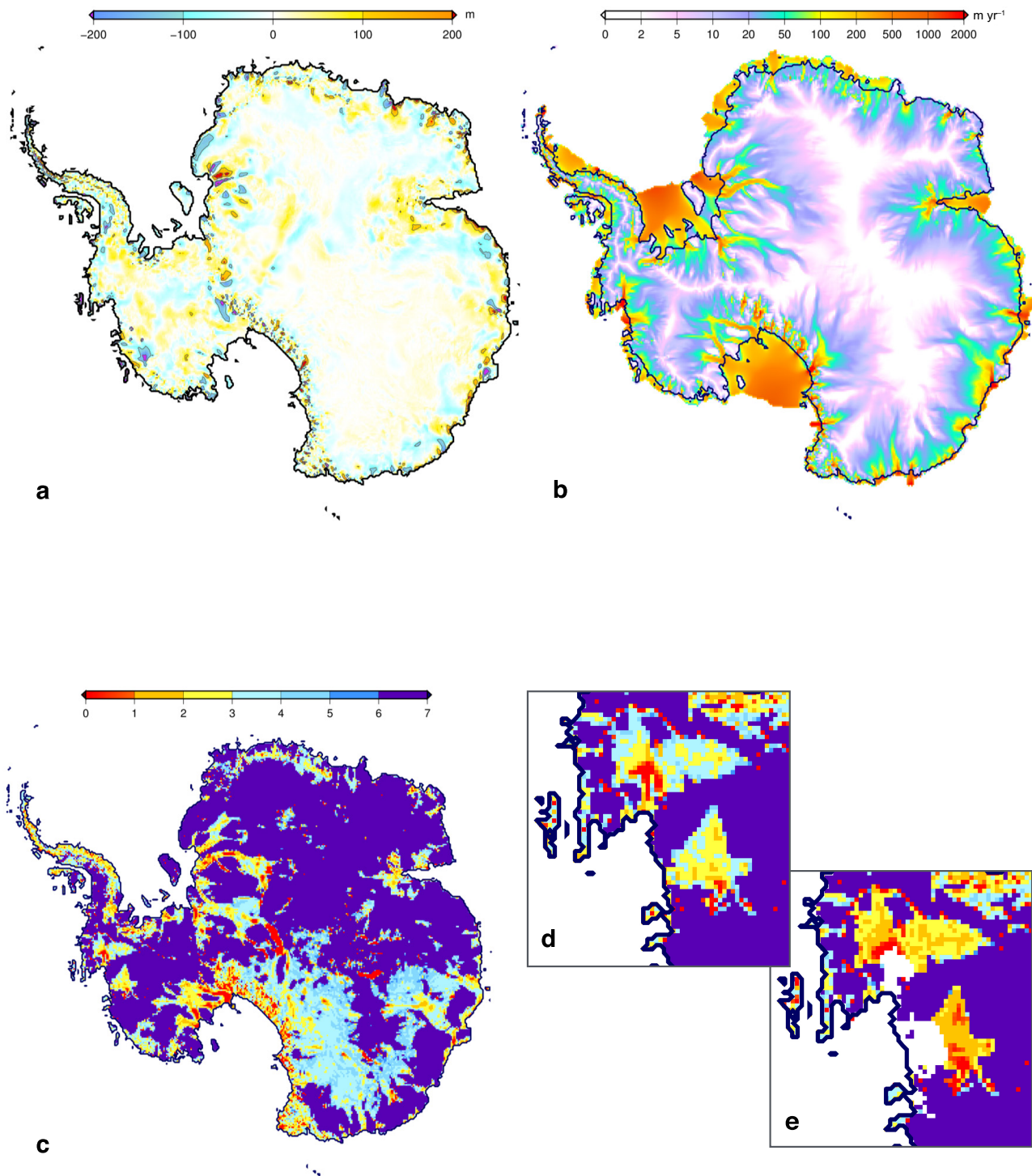
Extended Data Figure 2 | Initialization and basal friction evolution.
a–c, Initial values of the difference between simulated and observed surface elevation (**a**); velocities averaged over ice thickness (**b**); the logarithm of the initial effective basal friction coefficient, $\alpha = \log_{10}(\beta_1'$ $(\mathbf{x}; t = t_0))$ (**c**). **d**, As for **c**, showing the ASE. **e**, As for **d**, at 2200 in the plastic sliding law ensemble member that best matches present day ASE observations. See also Supplementary Information, section 1.5.

Extended Data Figure 3 | Projected grounding-line retreat and initial basal friction. a, b, Initial grounding line and map of α values (Extended Data Fig. 2) with retreat probability contours at 2200 for the Weddell Sea sector (**a**) and ASE (**b**): for example, there is an estimated 33% probability that grounding-line retreat will be less extensive than the 66% contour.
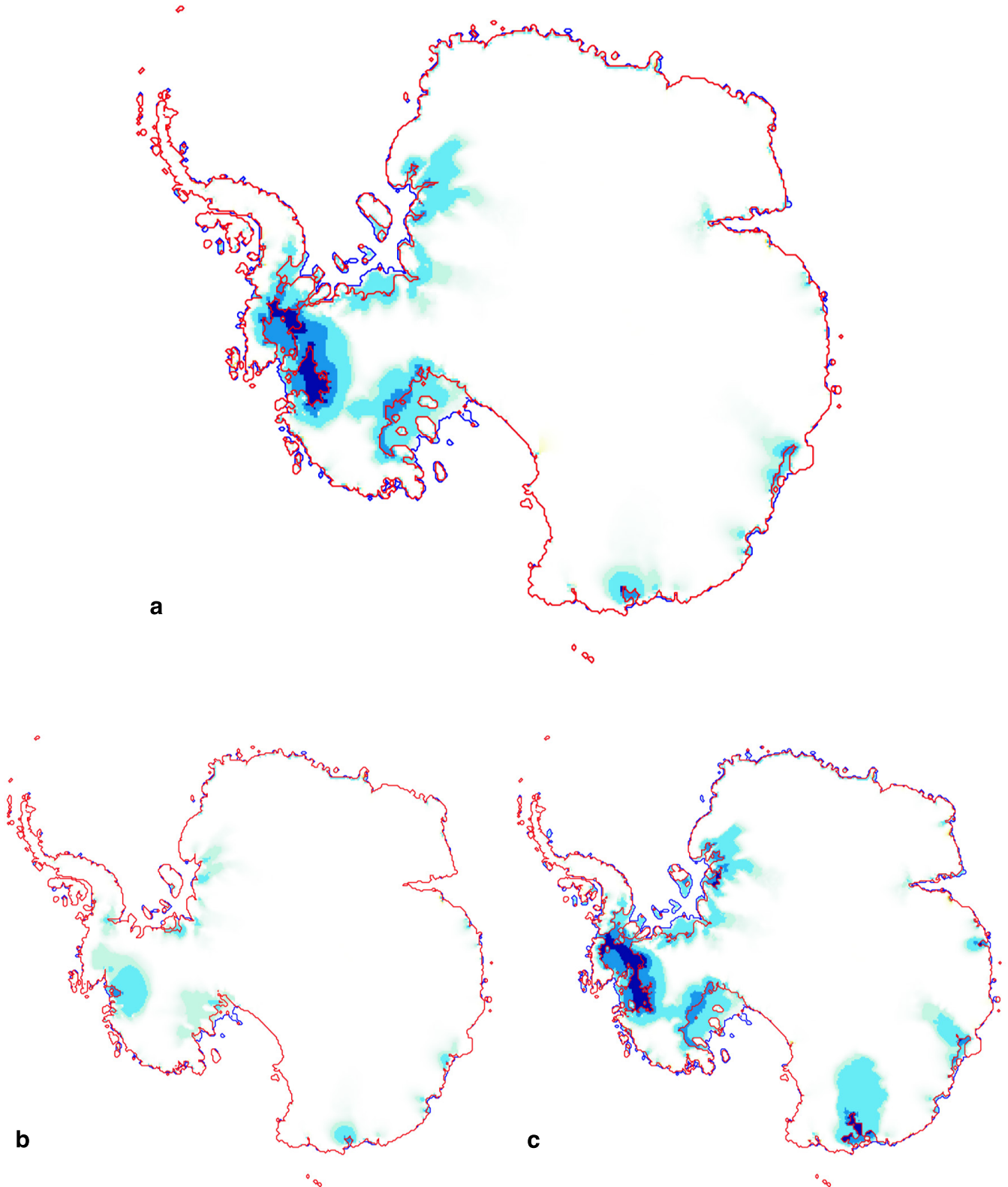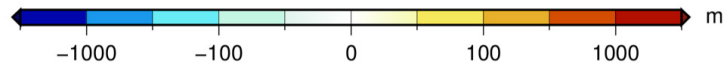
Extended Data Figure 4 | Ice dynamical conditions for retreat.
a–c, Surface elevation changes at 2200 in the ensemble member with maximum sea-level contribution at 2200 (plastic sliding law): standard settings (**a**); 'Schoof flux' condition off, thereby only allowing grounding-line retreat along strictly downsloping bedrock (**b**); 'no suction' check off, thereby allowing thinning due to grounding line retreat to occur faster than the theoretical limit (**c**). See also Supplementary Information, section 2.2.1.
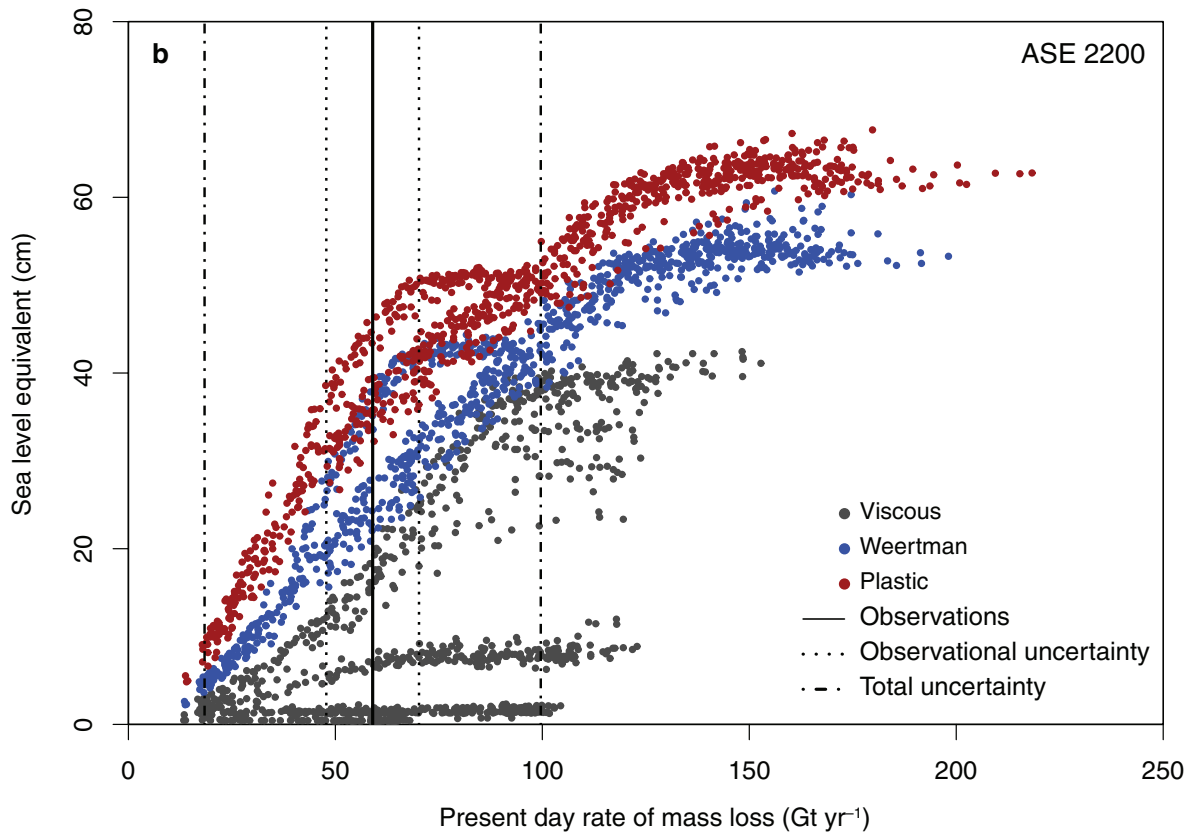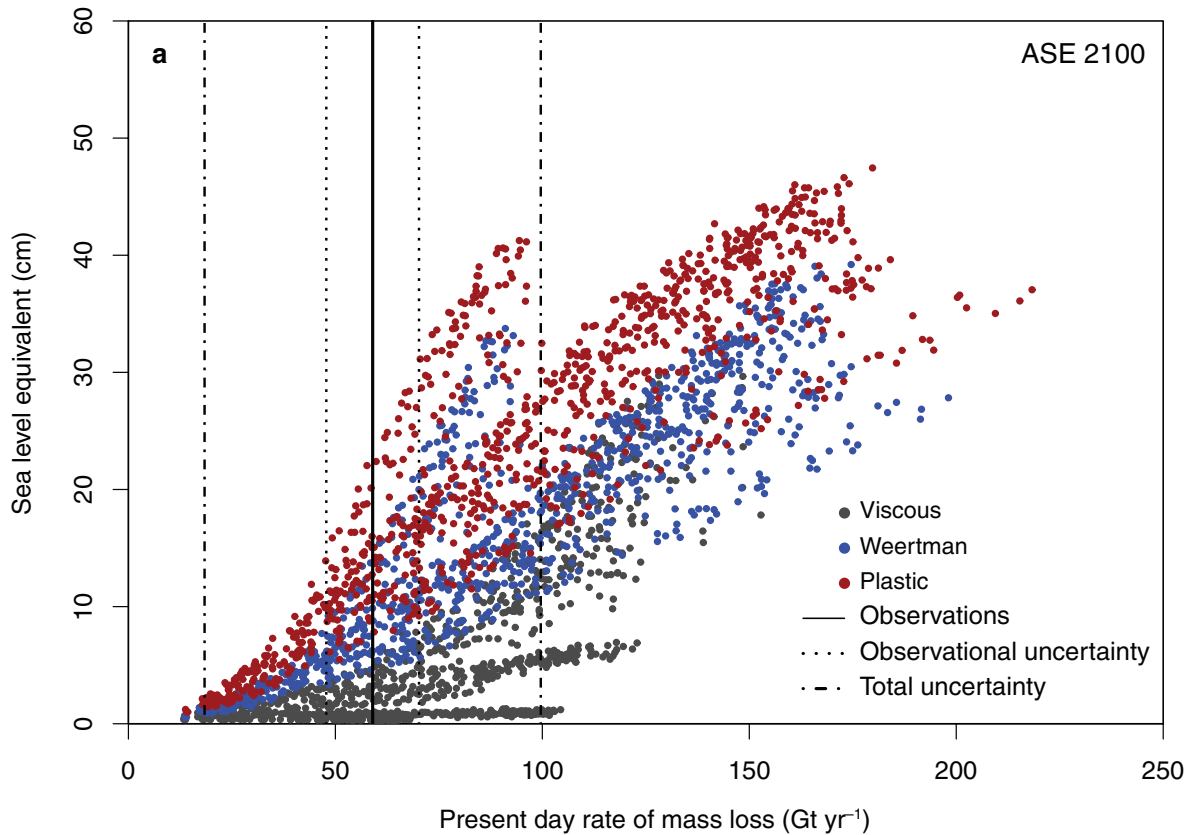
Extended Data Figure 5 | Relationship between present and future sea-level contributions from the Amundsen Sea. a, b, Dynamic mass losses in cm sea-level equivalent from the ASE at 2100 (**a**) and 2200 (**b**), as a function of present day mass loss in the same region. The branches arise from interactions between basal drag coefficient and friction law that produce different rates of, and impediments to, grounding-line retreat. The observed mass loss is shown, along with observational ($\pm 3\sigma_o$) and total ($\pm 3\sigma_t$) uncertainties (Supplementary Information, section 1.7).
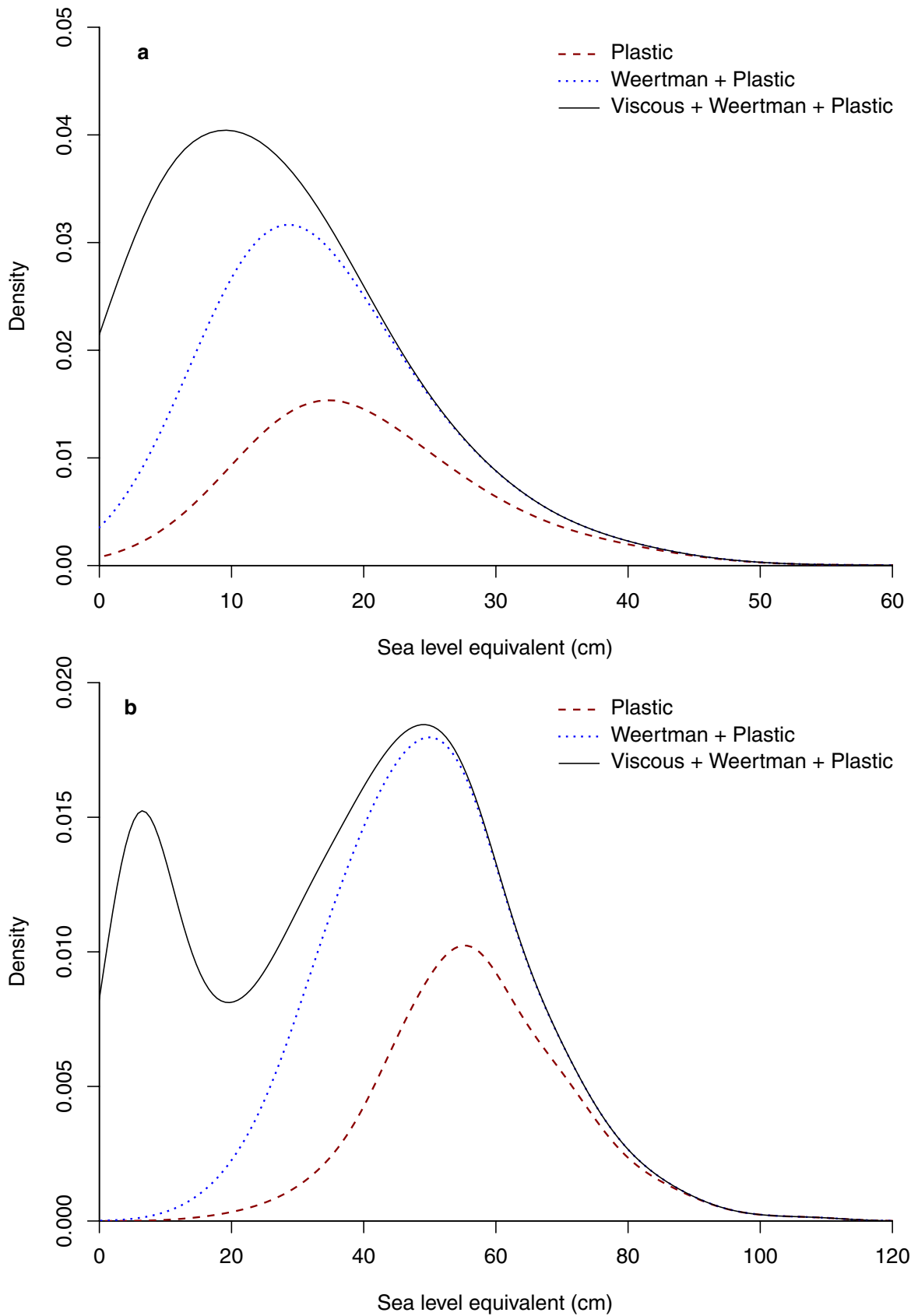
Extended Data Figure 6 | Contributions of each basal friction law. a, **b**, Probability distributions of Antarctic dynamic mass losses in cm sea-level equivalent at 2100 (**a**) and 2200 (**b**) (as in Fig. 2b), showing the cumulative contributions of the basal friction laws.
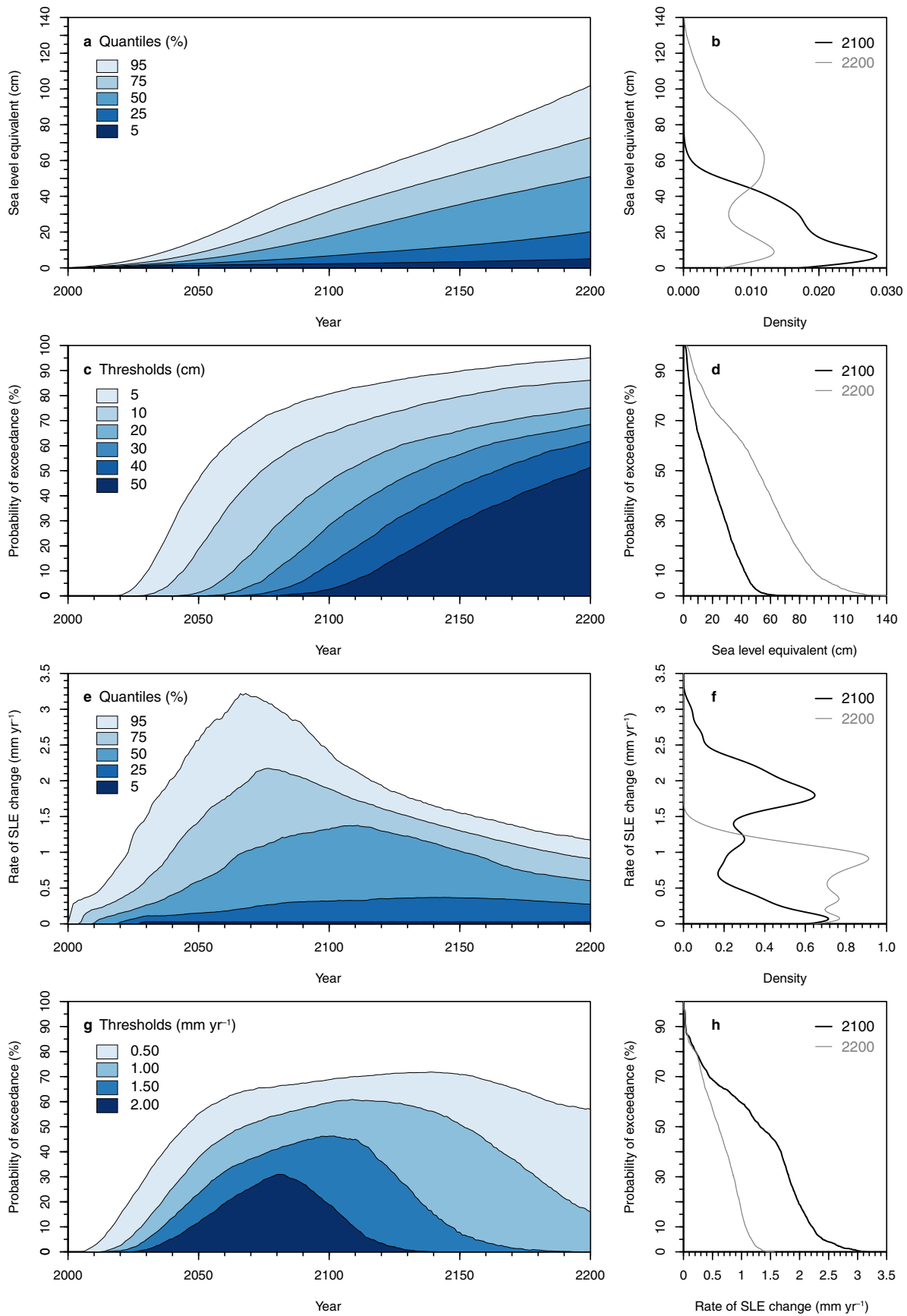
Extended Data Figure 7 | Uncalibrated projections. a–h, Prior (uncalibrated) projections of Antarctic dynamic mass losses in cm sea-level equivalent (**a–d**); rate of ASE dynamic mass losses in mm yr^{-1} sea-level equivalent (SLE) (**e–h**). Posterior (calibrated) projections are in Figs 2 and 3. See also Supplementary Information, section 1.7.
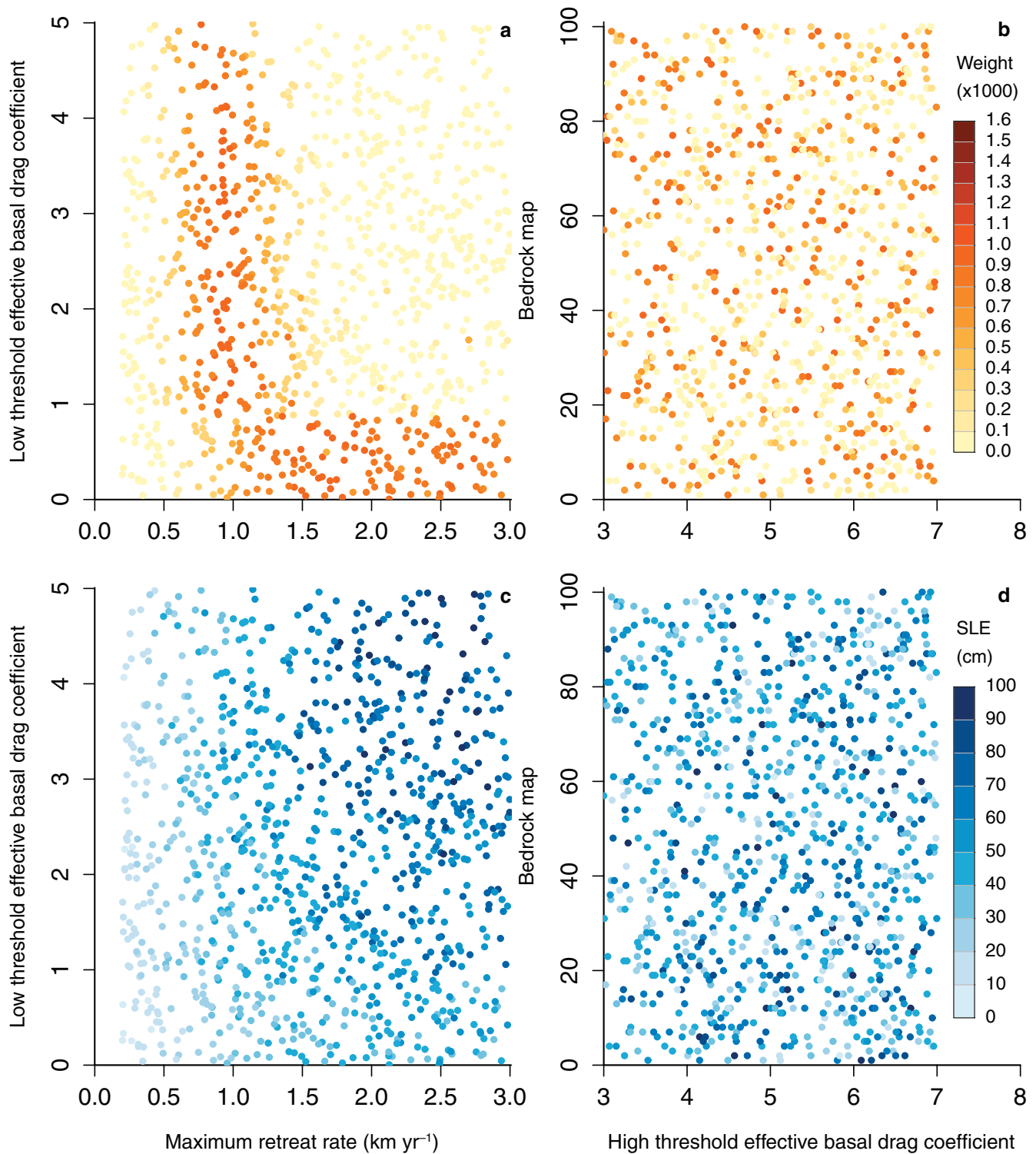
Extended Data Figure 8 | Parameter calibration and influence.
a, **b**, Weights for each of the 1,000 sub-ensemble parameter sets (averaged over basal friction laws) as a function of low threshold of effective basal drag coefficient (α_{low}) and maximum retreat rate (v_{max}) (**a**); bedrock map index and high threshold of effective basal drag coefficient (α_{high}) (**b**). Darker colours indicate values favoured by observational calibration. **c**, **d**, Uncalibrated dynamic mass losses at 2200 in cm sea-level equivalent (SLE) as functions of the same.
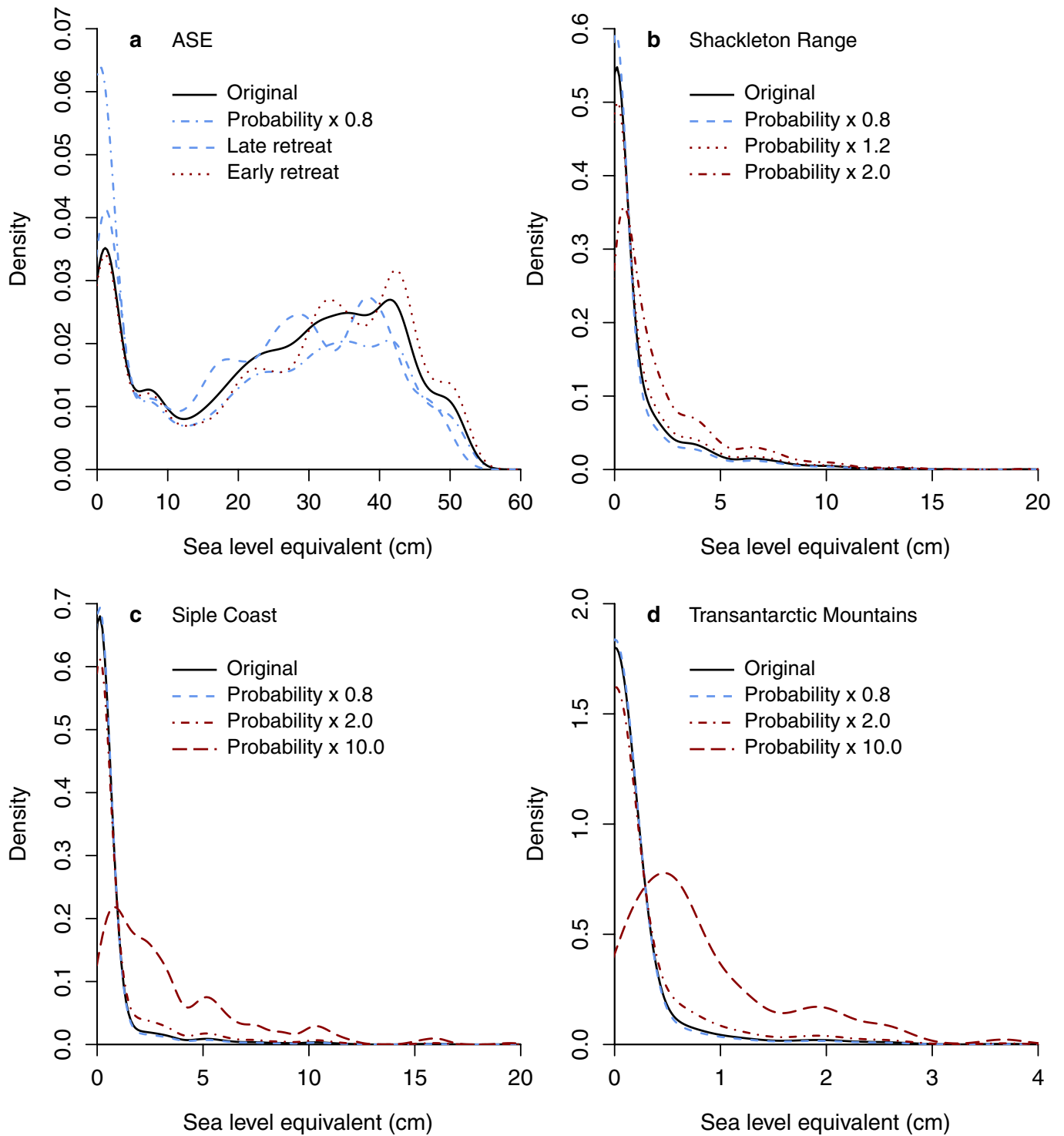
Extended Data Figure 9 | Sensitivity to retreat onset distributions.
a–d, Projections at 2200 estimated for four individual basins under different retreat onset scenarios. **a**, ASE: original; 'probability × 0.8', in which 20% of simulations are set to zero contribution; 'late retreat', in which all simulations begin retreating between 2020 and 2030; and 'early retreat', retreating between 2000 and 2010; **b**, Shackleton; **c**, Siple Coast; and **d**, Transantarctic Mountains: original, and onset probabilities adjusted by the factors shown. See also Supplementary Information, section 2.2.2.
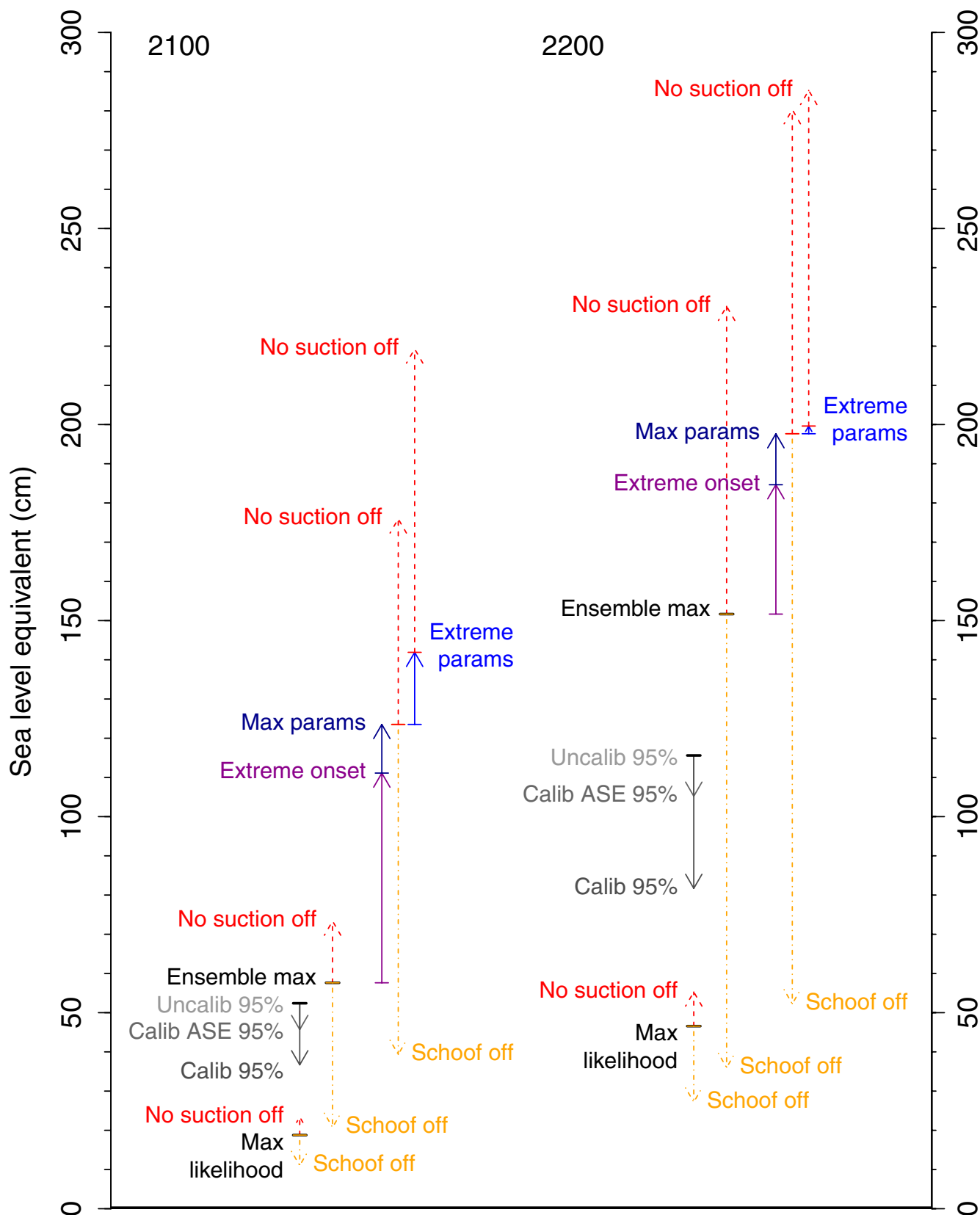
Extended Data Figure 10 | Sensitivity tests for plastic sliding law. Antarctic dynamic mass losses in cm sea-level equivalent under various conditions: 'Max likelihood', the plastic simulation that best matches present day ASE observations; 'Uncalib 95%' and 'Calib 95%', the plastic quantiles before and after calibration, respectively, and 'Calib ASE 95%', the estimate calibrating only the ASE; 'Ensemble max', the simulation with highest contribution at 2200; 'Extreme onset', the previous with all basins retreating from 2000 or 2020; 'Max params', the previous with retreat parameters at maximum values and 'Extreme params' at higher values; 'Schoof flux' and 'No suction' checks off (dashed to indicate that they are physically unrealistic). See also Supplementary Information, sections 2.2, 2.3.